Alexandria Engineering Journal (2021) 60, 3275–3293

HOSTED BY

ELSEVIER

Alexandria University

Alexandria Engineering Journal

www.elsevier.com/locate/aej
www.sciencedirect.com



Crane automation and mechanical damping methods



Serkan Beller [a,*], **Hakan Yavuz** [b,*]

[a] *İmamoğlu Technical Science College, Gas, and Fitting Technologies Department, Çukurova University, Adana, Turkey*
[b] *Faculty of Engineering, Mechanical Engineering Department, Çukurova University, Adana, Turkey*

Received 27 July 2020; revised 5 January 2021; accepted 25 January 2021

KEYWORDS

Automation;
Mechanical damping;
Simple pendulum;
Wind forces;
Neural networks;
Intelligent control

Abstract In recent years, the importance of automation systems in the industry has undergone a rapid development process, has started to be understood better and the need for a trained labor force has increased in the field. With the advances automation system, more tasks that are normally performed or controlled by humans are achived by machines or automatic systems. Thus, both faster production and higher production performances are achived by machine while labor is utilized other area where it is less hazardaous to human health. To operate such systems safely and economically, advanced control systems are needed. In this study, the transportation of a load with variable load and height have been automated by Zero Vibration (ZV) input shaping and Neural Network (NN) intelligent control methods in the Matlab/Simulink environment. In addition, the mechanical damping methods have been developed against external forces. It has been shown that this is necessary not only for positioning a load with minimum oscillation but also for balancing it against wind forces. The presented study provides theoretical analysis of the problem, related state of the art industrial applications, the results of the simulation and the experimental studies of the proposed techniques.

© 2021 THE AUTHORS. Published by Elsevier BV on behalf of Faculty of Engineering, Alexandria University. This is an open access article under the CC BY license (http://creativecommons.org/licenses/by/4.0/).

1. Introduction

In the world, especially after the 1980s, radical changes have occurred in the design and production of industrial systems and related products. With the advancement of technology in the developing and changing world markets, significant changes have occurred in the quality and functions of industrial systems. Product design, system dynamics, and intelligent control; observation, modeling and control of production processes, mobile robot systems, power electronics, microsystem design and applications, industrial control design, sensors and robot systems, image processing, artificial neural networks (ANNs), artificial intelligence and virtual reality, defense industry, automotive and textile areas are among the new fields of industrial automation [1].

The fast, standard, safe, and efficient production in competitive conditions has become a necessity in the global open mar-

* Corresponding authors at: Çukurova University, Faculty of Engineering and Architecture, Mechanical Engineering Department, 01330 Sarıçam, Adana, Turkey
E-mail addresses: sbeller@cu.edu.tr (S. Beller), hyavuz@cu.edu.tr (H. Yavuz).

Peer review under responsibility of Faculty of Engineering, Alexandria University.

https://doi.org/10.1016/j.aej.2021.01.048
1110-0168 © 2021 THE AUTHORS. Published by Elsevier BV on behalf of Faculty of Engineering, Alexandria University.
This is an open access article under the CC BY license (http://creativecommons.org/licenses/by/4.0/).

Nomenclature

DC	Direct current
RPA	Rotational pendulum absorber
CPR	Counts per revolution
RPM	Revolutions per minute
V	Volt
A	Amper
bit	Smallest data storage value
GHz	Gigahertz
MB	Megabyte
RAM	Work memory
AGV	Driverless transport systems
ARMG	Automated rail mounted gantry crane
GSU	Grab/ship unloader cranes
OHBC	Overhead bridge cranes
ZPMC	Shanghai zhenhua heavy industries company
COSCO	Shipping ports limited
ARTG	Automated rubber-tired gantry crane
PDS	Container position detection systems
TLS	Trim, list, and skew control
Grab cranes	A hoisting machine fitted with a clamshell
SND	Current trolley position
SNL	Load position

ket. The automation in the industry is certainly the answer to need. On the other hand, automation can be done not by a single device but by the collective operation of many control and automation technology units. So, it is possible to make production in the industry fast, standard, safe and efficient.

The automatic systems were also developed in commercial cranes too. One of them is the robotized cranes [2,3,4]. The automation applications are also frequently used in inverted pendulum applications [5–9]. For the system automation to take place, the system definition must be performed very well. For this, many studies have been carried out under the System Identification heading. The System identification (SI) uses some methods to construct mathematical models of dynamic systems. These methods make predictions between the signals at the input and output of a system. Thus, the behavior of existing structures is examined by recording the system input parameters and related output vibrations of the structures in separate time signals [10]. Also, the dynamic system output is mapped to the previous input and output values by mathematically by complex equations. Usually, this process is a complex one and no perfect match is guarantied. Hence, some intelligent control methods are proposed and used by researchers [11–14].

Following the creation of the mathematical model of the system for vibration analysis, differential equations (motion equations) that define the motion of the system are created using one of the methods available in the literature. Different methods can be used for creating equations of motion such as Newton's Second Law, Dynamic Equilibrium Method (d'Alembert Principle), Energy Method, Lagrange Method and so on. In this study, d'Alembert Principle is utilised. For many different systems, the dynamic model is best expressed in differential equation form. The easiest way to map the input-output relationships in term of control theory lagguage is to use a transfer function. The transfer function of a linear and time-independent differential equation is expressed as the ratio of Laplace transform of output to Laplace transform of input. Thus, differential equations that are difficult to solve in the time domain are converted into simpler algebraic equations that are easier to solve in the frequency domain [15]. In this study, while creating the transfer function of the pendulum test set, the system parameters were obtained instantly through the system in the Matlab/Simulink environment with the automation block.

It may not be possible to present the solutions to many engineering problems that we encounter today with simple mathematical expressions. The uneven geometry, the non-uniform load, and the nonlinear behavior of the materials prevent us from obtaining simple linear analytical solutions. In such cases, approximate solutions are made by dividing the problem into smaller parts. At this point, the finite element method (FEM) comes into play. Today the deficiencies of this method have been eliminated by the spectral element method (SEM) [16–22].

In this study, a control block that works with hybrid Artificial Neural Network (ANN) is developed for intelligent control of a simple pendulum. The input data required for system control of the pendulum is fitted with different weights at different heights and they are chosen to be constantly varying. In the determination of the data, the information obtained from instantly drawn graphs are used. Thus, the input data can be obtained more quickly without losing time with the calculation. With this input data, output analog signal values are generated in the intelligent control blocks. The aim is to move the load transferrred by the pendulum to the desired position in minimum oscillation levels by utilizing ZV input shaping and ANN control methods [23]. The ZV Shaper is a two-pulse open-loop control system. It is basically the Posicast control technique. The posicast control technique was developed in the late 1950s. It is a method of designing a control system using the mathematical model of dynamic systems performing damped oscillation expressed with a set of second-order differential equations. It is a method that completely eliminates dynamic system interactions without requiring any measurement or information other than the accurately determined parameters of the system model [15].

Earlier, many intelligent methods against external forces have been used for crane controls in [24–32]. In addition to intelligent methods, some mechanical damping methods have been developed too. Various mechanical damping methods are listed in Table 1. The active or passive dampers have been preferred to protect the systems against the effects of unwanted oscillations. In this study, by placing different types of pendulums on the top of the main pendulum, the model includes the wind forces that were not tried to be compansated in previous studies. The mechanical design of the system is also important in terms of energy savings. Here, the gravitational force is used for transforming it into a useful force to further reduce the

Table 1 Mechanical damping methods.

#	Ref.	Year	Damping Type	Purpose of Use	Benefits
1 1	[33]	2015	Coriolis damping	Payload sway reduction by spring and damper.	Load horizontal motion with the initial angle of −15 is reduced with 35.6%, for 15 with 44.1%, for −20 with 43.9%, for 20 with 49.0%. Load vertical motion with the initial angle of −15 is reduced with 35.1%, for 15 with 47.0%, for −20 with 46.4%, for 20 with 54.3%.
2	[34]	2015	Cable-passive damper system	Reduce the vibration of a four cable suspended crane spreader.	The suggested damping system can improve the X-offset reduction of the Zero Vibration Derivative (ZVD) input shaping method from 69% to 85%. The damper was designed for the spreader mass of 20 tons.
3	[35]	2007	Isolators	Increase the effectiveness of the anti- vibration.	The stored potential energy is the most major factor affecting the natural frequency. When the added systems are combined with the original insulation systems, building insulation systems with low natural frequencies are obtained.
4	[36]	2019	Moving mass	The asymptotic stability of a pendulum.	The moving mass is a mechanism for swing control of pendulums. Time-varying inertia, created by a mass sliding along with a rotating member, is associated with Coriolis forces.
5	[37]	2017	Semi-active vibration absorbers	Suppress large amplitude swings in container cranes.	The performance of a passive control system is largely influenced by the mass ratio $\rho = m/M$ as well as the tuning conditions. The dynamical response of a 40-ton container was evaluated while exposed to side winds. With three different (895, 450, 225 kg) absorbers the best performance was achieved by 895 kg.
6	[38]	1999	Mechanical filter	Suppressing of crane-load oscillations.	Both linear and non-linear dynamical systems corresponding to the systems with and without the filter have been examined. The active filter used for attenuating transient crane load oscillations besides steady-state oscillations too.
7	[39]	2019	Nonlinear absorber for passive cont.	Swing control of 2D freedom pendulum.	The pendulum was passively controlled by a non-linear absorber. The energy exchanges between the main oscillators and the nonlinear energy sink (NES) have been reported to be successful.
8	[40]	2019	Passive vibration absorber	Controlling of the vibration amplitude.	The dynamics of an oscillating rotary system subjected to external harmonic excitation were examined. The regulated mass damper was connected to the main system to prevent possible resonance. The damper mass has been shown to stabilize periodic motion asymptotically.
9	[41]	2019	Passive vibration absorber	Vibration suppression.	Passive vibration absorbers can be very effective if the excitation frequency is fixed and close to one of the system's resonance frequencies. For a DC fan, there is a 98% of reduction in vibration amplitude with the vibration absorber (16 Hz input and absorber designed for 16 Hz) attached. In contrast, there is an increase of 67% in vibration amplitude at a steady state. Because excitation was at 23 Hz and vibration absorber designed for 16 Hz.
10	[42]	2011	Mag. Lev. with an autoparametric vibration absorber	Reduction in the amplitude of primary resonance of a bar.	The reduction came true in the amplitude of primary resonance of a bar with magnets levitated above superconducting bulks by an attached pendulum. This kind of vibration absorber is useful for reducing the resonance of a high superconducting levitation system.
11	[43]	2011	Rotational pendulum vibration absorber	Neutralizing torsional disturbances.	The effectiveness of the semi-active vibration absorber was seen in experiments. The responses of the flexible plate with an idle RPA, an optimally tuned RPA, and an over-driven RPA were compared. When the RPA is activated (Rotational speed is 39 rad/s), the vibrations are sharply reduced. The fundamental component (10 Hz) is almost cleaned out. When the rotational speed is set at 50 rad/s, firstly structure vibrates, and an uncontrolled situation occurs.
12	[44]	2016	An adjustable pendulum with m mass	Reducing oscillations during earthquakes, winds at the buildings.	A multi-body dynamic simulation was compared with theoretical numerical results in a real case and the oscillations were significantly reduced. It is shown that the two heaviest pendulums (mass over 20% of the block mass) can prevent the rocking of the block, whereas without a pendulum the block would oscillate noticeably. Also, for a low mass pendulum (up to 20% of the block mass) no oscillations reduction occurs despite the pendulum length.

oscillation. The duration of oscillations was reduced by up to 80% thanks to active dampers. The fact that the mechanisms can move taking into account the wind direction also makes it an effective protection method against external disturbance effects. It is thought that this damping rate can be increased even more with intelligent control methods, electric motors, and various sensors. Mechanisms have been tried in both rope based and fixed bar pendulums. Also, as two different mini damping pendulums are used together, the compound pendulum was preferred as the definition. In this paper, section two occurs from the control chart, and equations of motion are presented. In section three, experiment studies and graphical results are evaluated. The section four presents the final conclusions.

2. Material and methods

2.1. Material

In this study, Makeblock mechanical fittings were preferred for the simple pendulum experiment setup. The other equipments used are Pololu 12 V brushed DC motor with integrated 48 CPR quadrature encoder (2250 RPM, 300 mA free-run) [45], Pololu simple high-power motor controller card 24V23A [46], Yumo rotary encoder – 200P/R (Quadrature) [47], Humusoft MF 634 multi-function I/O data acquisition card [48], Globex GXA1216 power source (12 V, 16.7A) and fully equipped computer (Windows 7, 64 bit, Intel Core i5-7500, 3.40 GHz, 16,384

MB RAM, AMD Radeon R7200 series graphics processor). The system was integrated with the Matlab/Simulink program. Matlab is used for recording of the experimental study results. Fig. 1 shows that the experimental setup very much similar to a typical gantry crane.

2.2. Methods

2.2.1. Automation block

If a pendulum leaves the free oscillation from a constant height, one can draw the amplitude time graph as shown in Fig. 2. The shape of the graph changes as different height and different amounts of weight are tested with the pendulum.

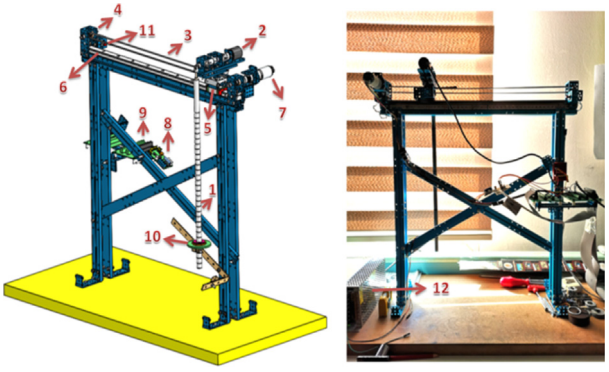

Fig.1 Simple pendulum; 1-pendulum bar, 2- encoder, 3- belt, 4-pulley, 5- trolley, 6- Mono Rail, 7- DC motor, 8- motor controller card, 9- data acquisition card slots, 10- variable weights, 11-stopper, 12- power supply.

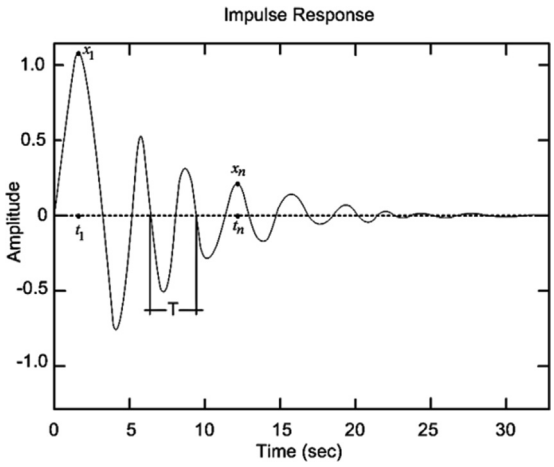

Fig.2 Pulse response to a damped system [15].

The natural frequency (ω_n) and damping ratio (ζ) can be determined from experimental measurements [15]. The measured value between the two peaks of the oscillation curve or the two zeros transition is period (T) of the damped oscillating system [15]. Also, T, ζ, weight (m), and load position (h) are the main parameter values. If these main parameter values are known then the other parameter values can be calculated.

The required data set for the control application consists of some system properties. The following terms are used respectively as input data (T, ζ, m, h) damped natural frequency (ω_d), ω_n, damping constant (c), spring constant (k), amplitude parameter (K), posicast input amplitudes (A_1, A_2). The more data input you have in training ANN, the more accurate data output values are achieved.

To find the ζ of the system given in Fig. 2; for $t = t_1$ time, swing amplitude x_1 and for $t_n = t_1 + (n-1)T$ time, swing amplitude x_n after measuring x_1 and x_2 amplitudes,

$$\zeta = \frac{\frac{1}{n-1}\ln\frac{x_1}{x_n}}{\sqrt{4\pi^2 + \left(\frac{1}{n-1}\ln\frac{x_1}{x_n}\right)^2}} \tag{2.1}$$

damped natural frequency (ω_d),

$$\omega_d = 2\pi\frac{1}{T} \tag{2.2}$$

natural frequency (ω_n),

$$\omega_n = \frac{\omega_d}{\sqrt{1-\zeta^2}} \tag{2.3}$$

If the ω_n and the ζ of the system are known, the share and the denominator of the transfer function can also be defined as [15].

If the unit pulse input is applied to the system as $R(s) = 1$,

$$\frac{Y(s)}{R(s)} = \frac{\omega_n^2}{s^2 + 2\zeta\omega_n s + \omega_n^2} \text{ and } Y(s) = \frac{\omega_n^2}{s^2 + 2\zeta\omega_n s + \omega_n^2} \tag{2.4}$$

damping constant (c),

$$c = 2\zeta\sqrt{km} \tag{2.5}$$

spring constant (k),

$$k = m\omega_n^2 \tag{2.6}$$

amplitude parameter (K),

$$K = e^{-\pi\zeta/\sqrt{1-\zeta^2}} \tag{2.7}$$

posicast input amplitudes (A_1, A_2),

$$A_1 = \frac{1}{1+e^{-\pi\zeta/\sqrt{1-\zeta^2}}} = \frac{1}{1+K} \tag{2.8}$$

$$A_2 = \frac{e^{-\pi\zeta/\sqrt{1-\zeta^2}}}{1+e^{-\pi\zeta/\sqrt{1-\zeta^2}}} = \frac{K}{1+K} \tag{2.9}$$

if the results are written in matrix form,

$$\begin{bmatrix} A_i \\ t_i \end{bmatrix} = \begin{bmatrix} \frac{1}{1+K} & \frac{K}{1+K} \\ 0 & \frac{\pi}{w_n\sqrt{1-\zeta^2}} \end{bmatrix} \tag{2.10}$$

The resulting ZV shaper ensures that no vibration occurs at the modeled frequency.

First of all, it is necessary to determine the working distance for a load to be transported by the ZV input shaping method. As shown in Fig. 3, the maximum oscillation angles that occur at the pendulum bar at this determined distance allows calculation of some parameters. The most important of these parameters are T and ζ. The period value in a pendulum varies according to the amount and height of the load installed on the pendulum bar. The calculation of these period values from oscillation graphs every time causes serious time losses. Another important parameter is the ζ. If the ζ is greater than one, then the system is over-damped. If it is equal to one, then the system is a critically damped type. If it has a value between zero and 1, then the system is lightly damped one. If it is equal to zero, then the system is an undamped type. To calculate the ζ of the system, the data in the oscillation graph must be calculated. This is also a time-consuming process. To prevent all these time losses and to run the system faster in automation, the automation block shown in Fig. 4 was developed in Matlab/Simulink environment.

To calculate the T, the loaded bar of the pendulum whose operating angle was already determined is released from a fixed point at the same angle. The information from the encoder is as shown in Fig. 5(a). This figure shows all the signals from the operating point to the stop position. These signals are initially filtered in the automation block. The objective here is to pass only the signals that belong to the operating angle and to block other signals.

As shown in Fig. 5(b), after the Edge Detector (ED) Block, countable instantaneous signals are generated for each peak value of these signals in the positive direction. The production times of these new signals give information about the times that each signal reaches its peak. One way of calculating the T is to take the difference between the times the signals reach the peaks [15]. The counter (C) block counts the total amount of these newly generated signals. The resulting total number will help us to calculate the ζ [15]. In the Subsystem (SS) block in Fig. 4, the ζ formula in Eq. (2.1) was applied. The total signal value counted in the Counter (C) block was used for the *n* value in this formula. This number will also be used to calculate the average T value. The T values between each signal that have reached the operating angle are different. As approach the damping point, these T values decrease slightly. With the Arithmetic Calculation Blocks in Fig. 4, the arithmetic mean is taken each time for these different T values. Thus, the ideal value of T can be calculated. The h and m quantities on which the load is suspended can be measured instantly with various sensors. Finally, the main parameters required for intelligent control methods are obtained. With these parameters, the total number of data entered in the Intelligent Controller Blocks in Fig. 4 is increased to eleven. Afterward, the load is brought to the desired position with minimum oscillation thanks to two pulse signals applied at certain times to the pendulum by artificial intelligence methods.

2.2.2. Mechanical damping

As mentioned in the second section, a large number of studies have focused on keeping a pendulum in the balance against external forces. In this study, some mechanical methods are used as shown in Fig. 6. Mini pendulums are placed on the main pendulum bar to prevent unnecessary oscillation from outside. These mini pendulums are sometimes tested to creating momentum in the same direction with the main pendulum and sometimes in opposite directions. If a load to the mini pendulums' arms are not added, the moment is formed in the same direction as the main pendulum rod. If a load to those arms are added then it is seen that momentum occurs in the opposite direction according to the main pendulum rod due to the grav-

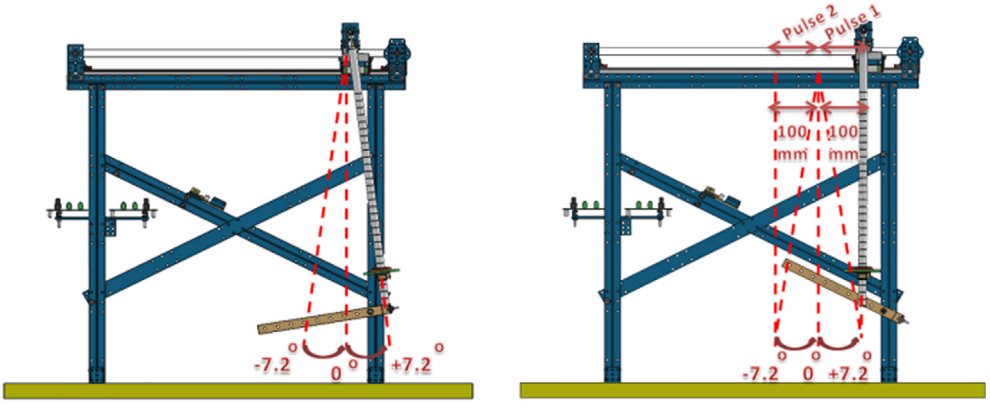

Fig.3 Simple pendulum; a) Movement angles b) Movement distances.

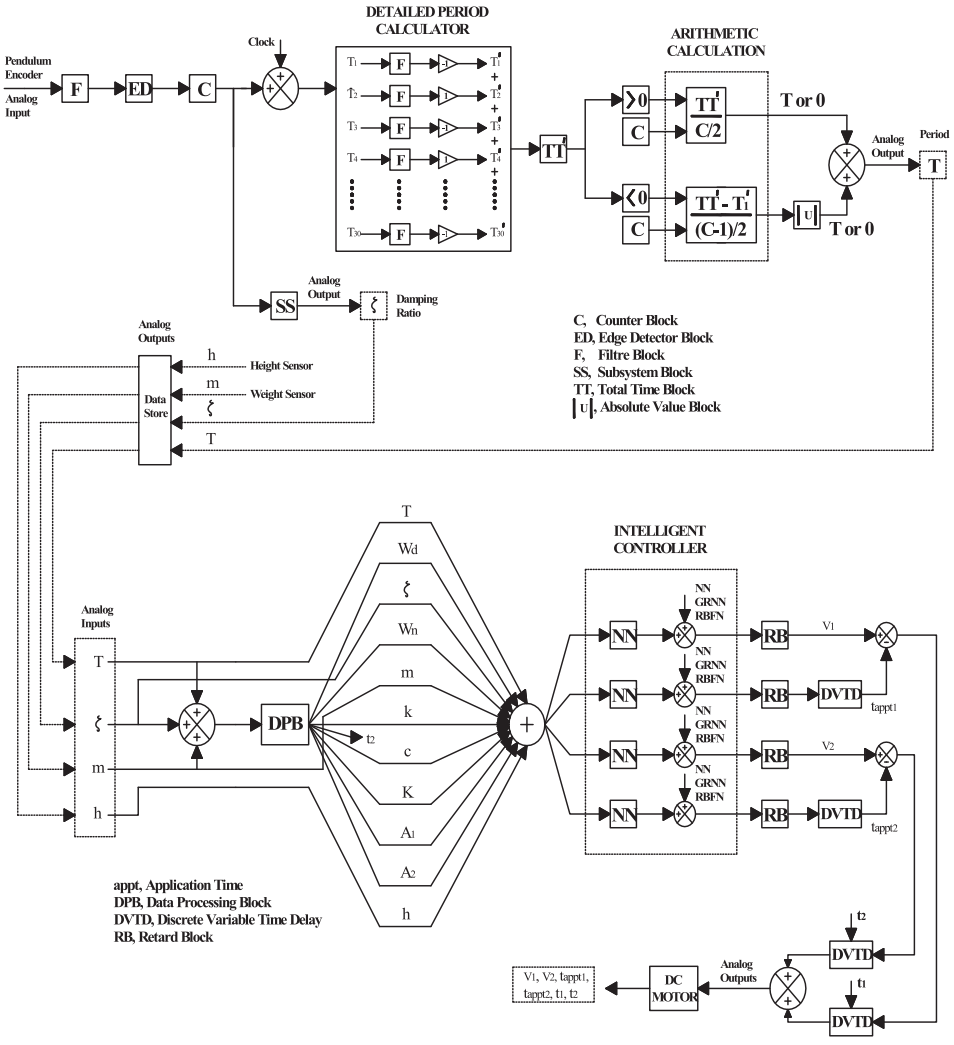

Fig.4 Automation block.

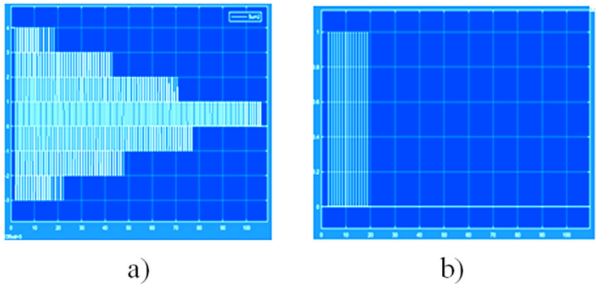

Fig.5 a) Pendulum oscillation graph b) Instant time measurement signals.

ity effect. All of these tests were carried out on both pendulums with a steel rod and the corded pendulum. Although the design of the mini pendulum changes in both pendulum types, rotary encoders are added to take the necessary measurements. Meanwhile, thanks to the mini corded pendulum, the number of ropes in the main pendulum has increased to three. In later studies, these two different pendulum types were combined to form a compound pendulum. The reason is that when more loads are added to the mini pendulums' arms, then there is need to add the more new loads on the opposite sides to keep the main pendulum rod in balance. The compound pendulum design has been tried instead of loading so many loads into the main system. With this method, both the overload was waived and a more effective opposite momentum was obtained. This compound pendulum has been tested both in steel rod pendulum and corded pendulum. Also, the oscillation of the main pendulum, as well as oscillations of the mini and compound pendulums are measured by two rotary encoders Figs. 6–10.

2.2.3. Equations of motion

In this study, the d'Alembert Principle, the dynamic equilibrium method [49,50,51], was used when creating the equations of motion.

$$\tau = F.d \text{ and } \sum M_0 = 0, \sum F = 0$$

For recall torque at the **Position I**;

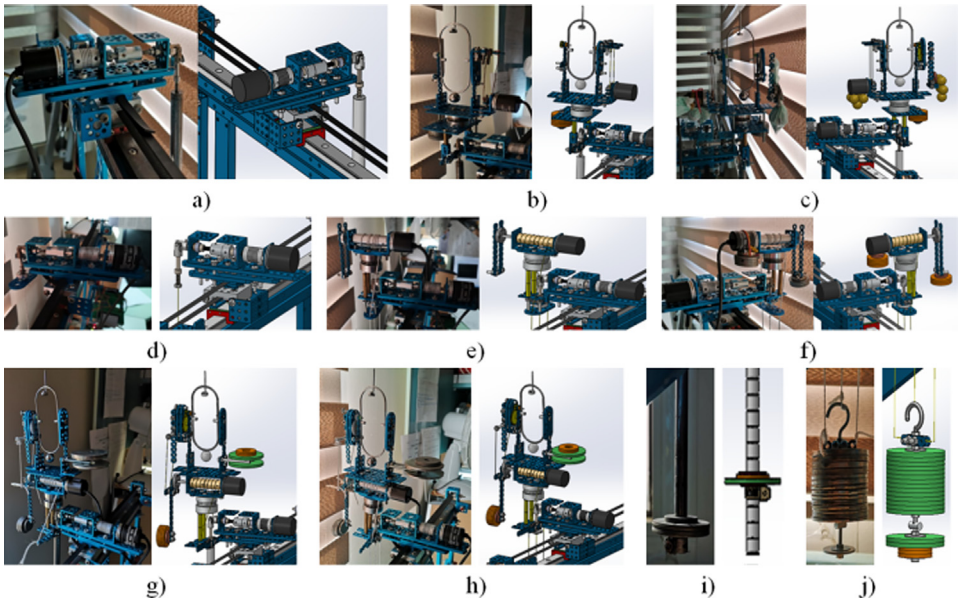

Fig.6 a) Simple pendulum with a steel rod b) Simple pendulum with a balancer mini pendulum without load c) Simple pendulum with a loaded balancer mini pendulum d) Simple pendulum with a rope e) Simple corded pendulum with a balancer mini pendulum without load f) Simple corded pendulum with a loaded balancer mini pendulum g) Compound (With two mini pendulum) pendulum with two rope and one steel rod h) Compound pendulum with three rope i) Pendulum steel rod with different loads j) Corded pendulum with different loads.

$$\tau = -m_1.g.\sin\theta.(L_1/2 + L_2) - m_2.g.\sin\theta.(L_2/2) + m_3.g.sin\theta.(L_3/2) + (m_4 + m_5 + m_6).g.cos\alpha.sin(\theta - \alpha).(L_3) \quad (2.11)$$

The equation between torque (τ) and moment of inertia (I);

$$\tau = I.\alpha = I.\frac{d^2\theta}{dt^2} \text{ and for small vibrations;} \quad (2.12)$$

Sin θ ≈ θ, and Sin (θ-α) ≈ (θ-α)
Motion equation;

$$\frac{d^2\theta}{dt^2} + \frac{m_1.g.(L_1/2 + L_2) + m_2.g.(L_2/2) - m_3.g.(L_3/2) - (m_4 + m_5 + m_6).g.\cos\alpha.(L_3)}{I}.\theta + \frac{(m_4 + m_5 + m_6).g.\cos\alpha.(L_3)}{I}.\alpha = 0 \quad (2.13)$$

Moment of inertia;

$$I = \frac{1}{12}.(m_1 + m_2 + m_3).(L_1 + L_2 + L_3)^2 + (m_1 + m_2 + m_3).d^2 + (m_4 + m_5 + m_6).(L_3)^2 \quad (2.14)$$

For the **Position II**;
Motion equation;

$$\frac{d^2\theta}{dt^2} + \frac{m_1.g.(L_1/2+L_2)+m_2.g.(L_2/2)-m_3.g.(L_3/2)-(m_4+m_5).g.\cos\alpha.(L_3-0{,}015m)+(m_6+m_7+m_8).g.\cos\beta.2{,}77.(L_3)}{I}.\theta + \frac{(m_4 + m_5).g.cos\alpha.(L_3 - 0,015m) - (m_6 + m_7 + m_8).g.cos\beta.2,77.(L_3)}{I}.\alpha = 0 \quad (2.15)$$

Moment of inertia;

$$I = \frac{1}{12}.(m_1+m_2+m_3).(L_1+L_2+L_3)^2 + (m_1+m_2+m_3).d^2 + (m_4+m_5).(L_3-0,015m)^2 + (m_6+m_7+m_8).(L_3)^2$$

For the **Position III**;
Motion equation;

$$\frac{d^2\theta}{dt^2} + \frac{m_1.g.(L_1+L_2+k)+m_2.g.(L_2/2)-m_3.g.(L_3/2)-m_4.g.(L_3/2)}{I}.\theta = 0 \quad (2.17)$$

Moment of inertia;

$$I = m_1.(L_1+L_2+k)^2 + \frac{1}{12}.(m_2+m_3+m_4).(L_2+L_3)^2 + (m_2+m_3+m_4).d^2 \quad (2.18)$$

For the **Position IV**;
Motion equation;

$$\frac{d^2\theta}{dt^2} + \frac{m_1.g.(L_1+L_2+k)+m_2.g.(L_2/2)-m_3.g.(L_3/2)-(m_4+m_5).g.\cos\alpha.(L_3)}{I}.\theta + \frac{(m_4+m_5).g.cos\alpha.(L_3)}{I}.\alpha = 0$$

Moment of inertia;

$$I = m_1.(L_1+L_2+k)^2 + \frac{1}{12}.(m_2+m_3).(L_2+L_3)^2 + (m_2+m_3).d^2 + (m_4+m_5).(L_3)^2 \quad (2.20)$$

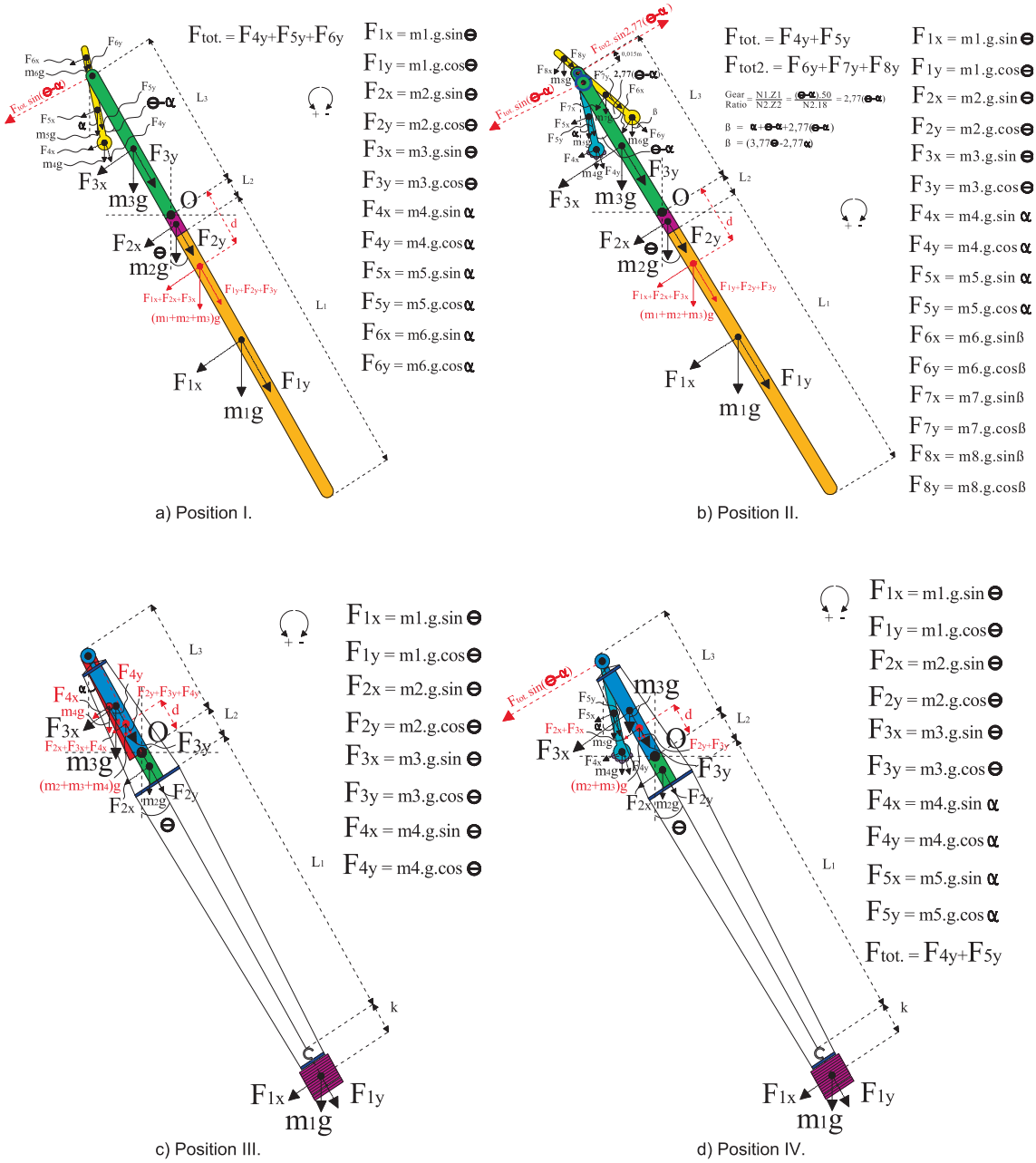

Fig.7 Free body diagrams; Pos. I, Pos. II, Pos. III, Pos. IV.

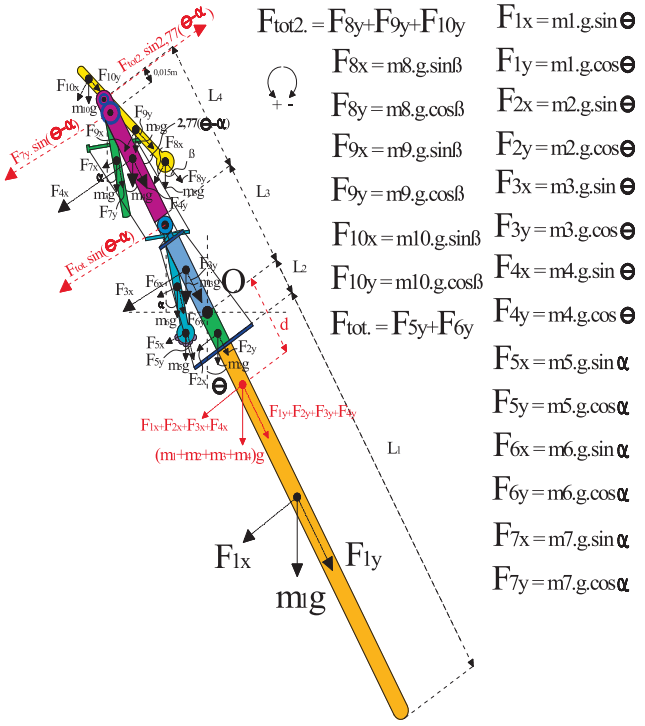

Fig.8 Position V. (Simple pendulum with compound pendulum and steel rod.)

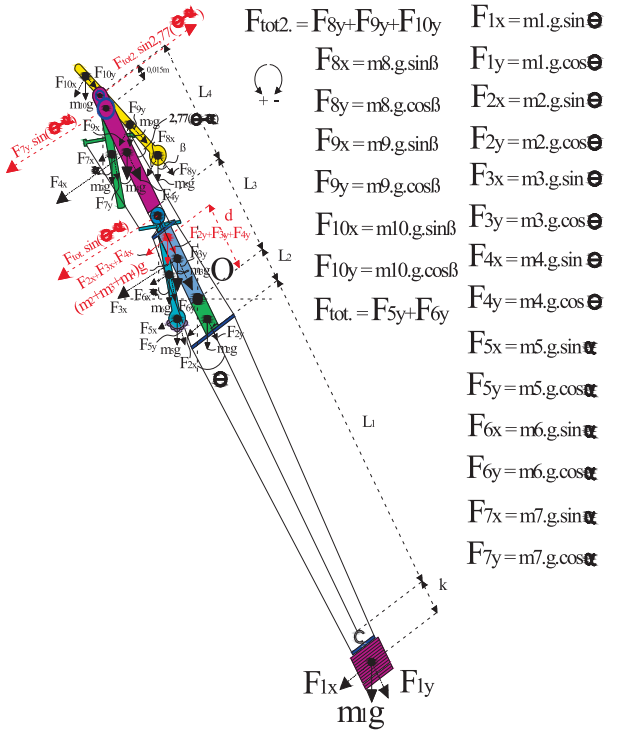

Fig.9 Position VI. (Simple pendulum with compound pendulum and rope.)

For the **Position V**;
Motion equation;

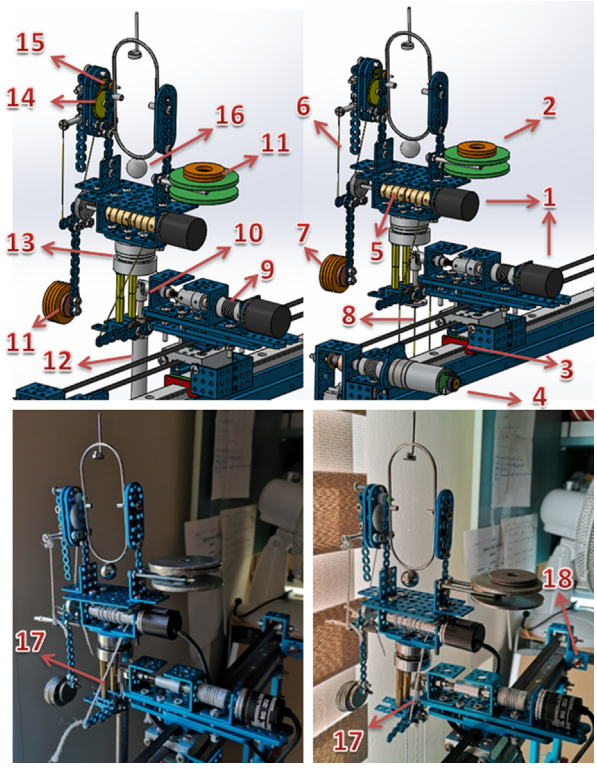

Fig.10 Compound pendulum: 1- Rotary encoder, 2- Balancing weights, 3- Trolley, 4- DC motor, 5- Drum 6- Connection rope between arms, 7- Pendulum arm weights, 8- Main rope, 9- Flexible coupling 10- Joint 4x4 mm, 11- Magnet, 12- Steel Rod, 13- Ball bearing rotary table D34x24 mm, 14- Big plastic gear (D25mm, 50 teeth), 15- Small plastic gear (D10 mm, 18 teeth), 16- Mini pendulum mace, 17- Supporting rope, 18- Stopper.

$$\frac{d^2\theta}{dt^2}+\frac{m_1.g.(L_1/2+L_2)+m_2.g.(L_2/2)-m_3.g.(L_3/2)-m_4.g.(L_4/2+L_3)-(m_5+m_6).g.\cos\alpha.(L_3)}{I}$$
$$-\frac{m_7.g.\cos\alpha.(L_4-0{,}015m+L_3)-(m_8+m_9+m_{10}).g.\cos\beta.2{,}77(L_4+L_3)}{I}.\theta$$
$$+\frac{(m_5+m_6).g.\cos\alpha.(L_3)+m_7.g.\cos\alpha.(L_4-0{,}015m+L_3)-(m_8+m_9+m_{10}).g.\cos\beta.2{,}77(L_4+L_3)}{I}.\alpha=0 \quad (2.21)$$

Moment of inertia;

$$I=\tfrac{1}{12}.(m_1+m_2+m_3+m_4).(L_1+L_2+L_3+L_4)^2$$
$$+(m_1+m_2+m_3+m_4).d^2+(m_5+m_6).(L_3)^2$$
$$+m_7.(L_4-0{,}015m+L_3)^2+(m_8+m_9+m_{10}).(L_4+L_3)^2 \quad (2.22)$$

For the **Position VI**;
Motion equation;

$$\frac{d^2\theta}{dt^2}+\frac{m_1.g.(L_1+L_2+k)+m_2.g.(L_2/2)-m_3.g.(L_3/2)-m_4.g.(L_4/2+L_3)-(m_5+m_6).g.\cos\alpha.(L_3)}{I}$$
$$-\frac{m_7.g.\cos\alpha.(L_4-0{,}015m+L_3)-(m_8+m_9+m_{10}).g.\cos\beta.2{,}77(L_4+L_3)}{I}.\theta \quad (2.23)$$
$$+\frac{(m_5+m_6).g.\cos\alpha.(L_3)+m_7.g.\cos\alpha.(L_4-0{,}015m+L_3)-(m_8+m_9+m_{10}).g.\cos\beta.2{,}77(L_4+L_3)}{I}.\alpha=0$$

Moment of inertia;

$$I=m_1.(L_1+L_2+k)^2+\tfrac{1}{12}.(m_2+m_3+m_4).(L_2+L_3+L_4)^2$$
$$+(m_2+m_3+m_4).(d)^2$$
$$+(m_5+m_6).(L_3)^2+m_7.(L_4-0{,}015m+L_3)^2$$
$$+(m_8+m_9+m_{10}).(L_4+L_3)^2 \quad (2.24)$$

The parameter data used in the calculations are shown in Table 2.

3. Experiment studies

3.1. Oscillation tests of pendulum with a steel rod

As seen in Fig. 11, as the damping method changes, the number and frequency of oscillation signals begin to change. The more successful the damping of the pendulum, the smaller the number and frequency of oscillation signals. As shown in Fig. 12(a), the most successful work here was with balancing the mini pendulum and loaded position. This success has been proven in three different study angles. In Fig. 11, only the data on the largest angles are presented. In this successful method, the oscillating mace in the mini pendulum moves in the same direction as the main pendulum bar, while the mini pendulum arm with its weight moves in the opposite direction to the main pendulum. The reason for this movement is the force of gravity. Here, the mini pendulum mace is opened from the mini pendulum at an angle greater than the weighted mini pendulums' main arm.

Thus, the damping moment effect on the main pendulum arm is greater. The main reason for this movement is that a

Table 2 Parameters of the positions.

	Pos. I	Pos. II	Pos. III	Pos. IV	Pos. V	Pos. VI
m_1(g)	370	370	841	841	370	841
m_2(g)	18,5	18,5	30	30	18,5	30
m_3(g)	311,5	334,5	159,5	247,5	164,5	164,5
m_4(g)	15	138	18	67	248	230
m_5(g)	7	34	—	18	85	88
m_6(g)	8	15	—	—	5	5
m_7(g)	—	7	—	—	5	5
m_8(g)	—	8	—	—	15	15
m_9(g)	—	—	—	—	7	7
m_{10}(g)	—	—	—	—	8	8
L_1(mm)	425	425	330	330	425	330
L_2(mm)	40	40	40	40	40	40
L_3(mm)	170	170	65	65	65	65
L_4(mm)	—	—	—	—	100	100
k(mm)	—	—	65	65	—	65
d(mm)	≈96,17 mm	≈90,40	≈22,77	≈29,05	≈77,40	≈69,04
$\theta(^0)$	21,6	21,6	25,2	25,2	21,6	25,2
$\alpha(^0)$	10,8	16,4	25,2	16,2	21,6	25,2
$\beta(^0)$	—	36	—	—	21,6	25,2
g(m/s^2)	9,81	9,81	9,81	9,81	9,81	9,81

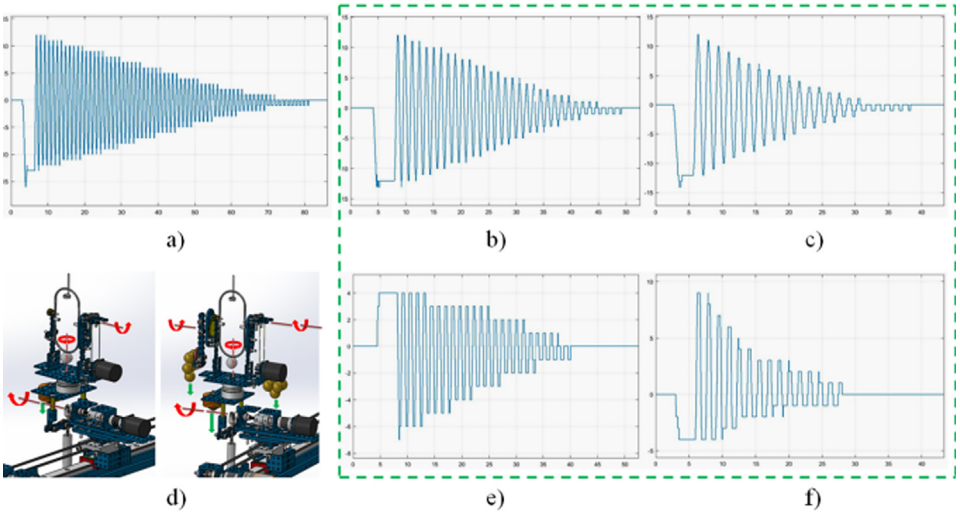

Fig.11 The main pendulum with 21.6°; a) no mini pendulum and no loads b) with mini pendulum and no loads c) with mini pendulum and loads, d) Balancer mini pendulum (With 21.6° main pendulum); e) with no loads, f) with loads.

gear group is located between the two mechanisms. The gear ratio is about 50/18. At the same time, the oscillation of the extra weights added to the system creates a damping effect too. As a result, this weight is added to a position higher than the peak of the main pendulum.

Fig. 11 (c) and (f) show oscillation graphs of both pendulums simultaneously. According to these graphs, the oscillations of both pendulums are in the same direction too. The encoder in the mini pendulum depends on the swing with the mace. The oscillation graphics of the main pendulum and mini pendulum are obtained instantly utilizing two encoders.

3.2. Oscillation tests of pendulum with a rope

Fig. 13 shows different oscillation graphs with different damping dampers. These graphs observed in the test of the largest

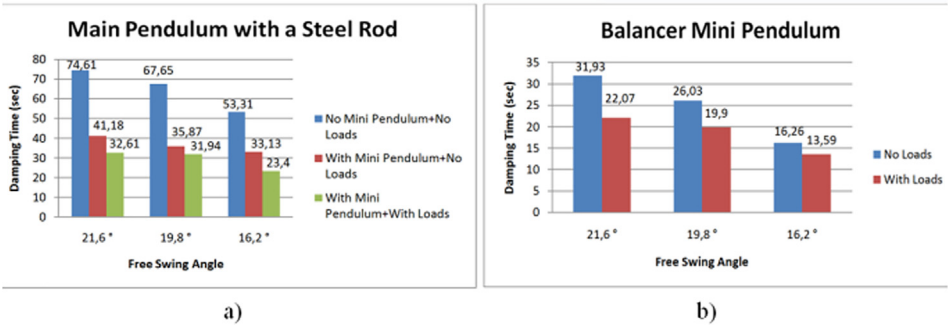

a) b)

Fig.12 a) Damping times of the main pendulum with a steel rod at the different conditions and angles b) Damping times of balancer mini pendulum at the different conditions and angles.

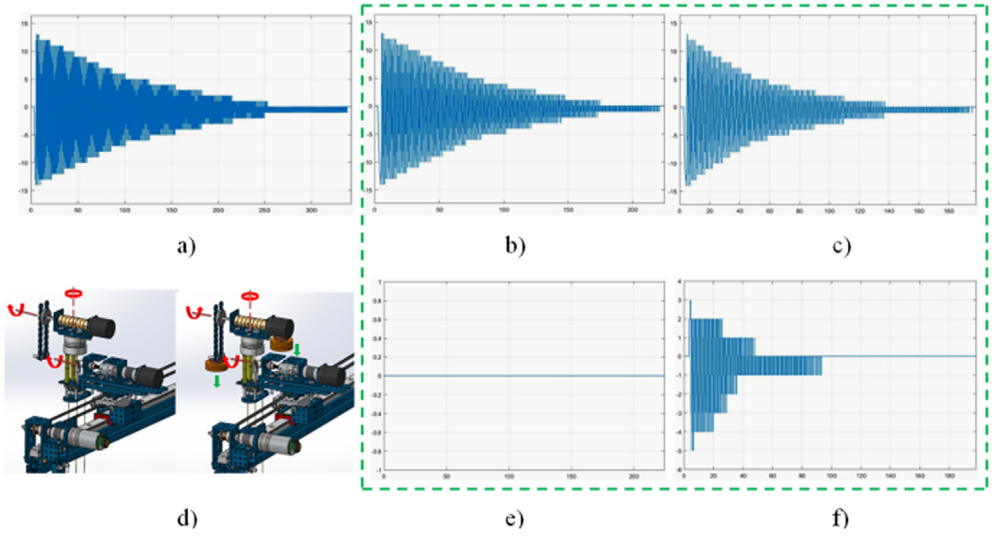

Fig.13 The main pendulum with 25.2°; a) no corded mini pendulum and no loads b) with corded mini pendulum and no loads c) with corded mini pendulum and loads, d) Balancer corded mini pendulum (With 25.2° main pendulum); e) with no loads, f) with loads.

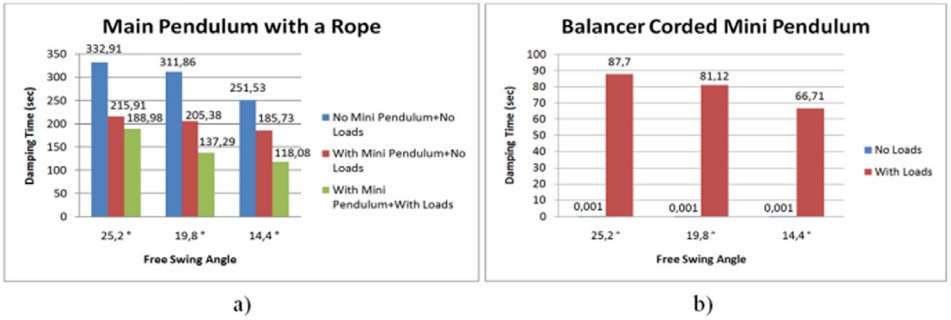

a) b)

Fig.14 a) Damping times of the main pendulum with a rope at the different conditions and angles b) Damping times of balancer corded mini pendulum at the different conditions and angles.

swing angle as shown in Fig. 14(a). Here oscillation signals are very close to each other. This is due to the length of the crane rope and the amount of load lifted. The smallest amplitude of oscillation is shown in Fig. 13(c). Here the corded mini pendulum was used with loads in Fig. 13(f) to reduce oscillations. When term "loads", indicates the weights added to the arm of the corded mini pendulum. With these weights, the mini pendulum can have a slowing effect against the main pendulum movement. Also, increasing the number of ropes from one to three provides an important advantage in controlling the suspended weight. Of course, the tension value of the two ropes added later to the system is also an important factor in damping. There will be changes in the oscillation times of the main pendulum according to this amount of tension.

As seen in Fig. 13(f), the corded mini pendulum has an oscillation between certain angles. Also, when added weights to the arm of the corded mini pendulum, it is necessary to add weights to the opposite side so that the main pendulum can be stabilized. These additional weights consequently affect the main pendulum damping time as it is placed on the main pendulum. In this study, the oscillation graphics of the main pendulum and corded mini pendulum are measured at simultaneously utilizing two encoders.

3.3. Oscillation tests of compound pendulum with a steel rod

The tests with weights applied to the mini pendulum arm proved to be more successful. Because the mini pendulum was more successful in oscillation damping by moving in the opposite direction to the main pendulum oscillation. To further increase the damping, these two mini pendulum styles were combined and some trials were performed. The two ropes are added to the system for oscillation control at the main pendulum with a steel bar. With addition of these, it is aimed at creating a forces in the opposite direction to main oscillation. According to the results presented in Fig. 16(a), the oscillation times of the main pendulum with a compound pendulum can be reduced by up to eighty percent (80%). During the tests, the pendulum mace moved very little. These values were below $+0.36°/-0.36°$ degrees. Since the pulse value of the encoders is 200 units, these oscillation values could not be reflected in the graphs as shown in Fig. 15(d,e,f).

Furthermore, the balancing weights above the peak of the main pendulum also used to damp the oscillations. The compound pendulum performance was then tested with ten different weights and at three different angles. The test results are presented in Fig. 16(b). All graphic results can be seen at the

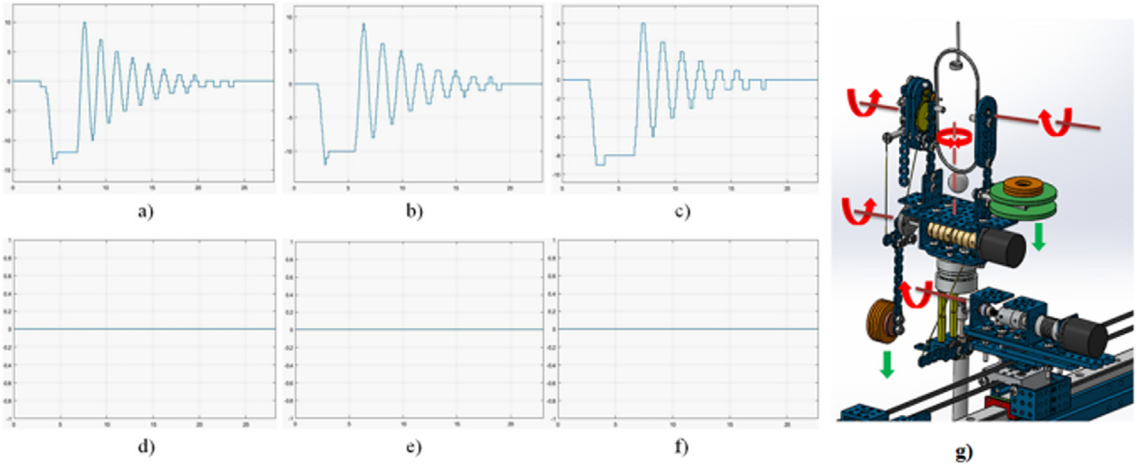

Fig.15 The main pendulum with a steel rod and a compound pendulum at the; a) 21.6° b) 19.8° c) 16.2°, Compound pendulum at the; d) 21.6° e) 19.8° f) 16.2°, g) The main pendulum with compound pendulum.

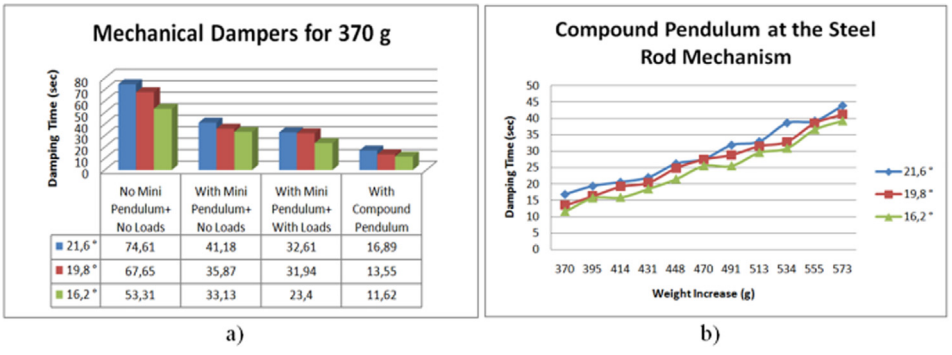

Fig.16 a) Damping times of the main pendulum with a steel rod at the different conditions and angles b) Damping times of the main pendulum with a steel rod and a compound pendulum with different weights and angles.

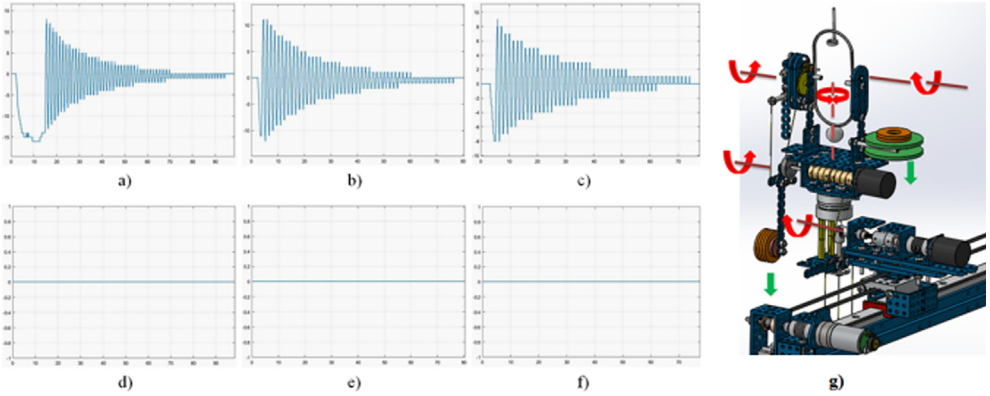

Fig.17 The main pendulum with a rope and a compound pendulum at the; a) 25.2° b) 19.8° c) 14.4°, Compound pendulum at the; d) 25.2° e) 19.8° f) 14.4°, g) The main pendulum with compound pendulum.

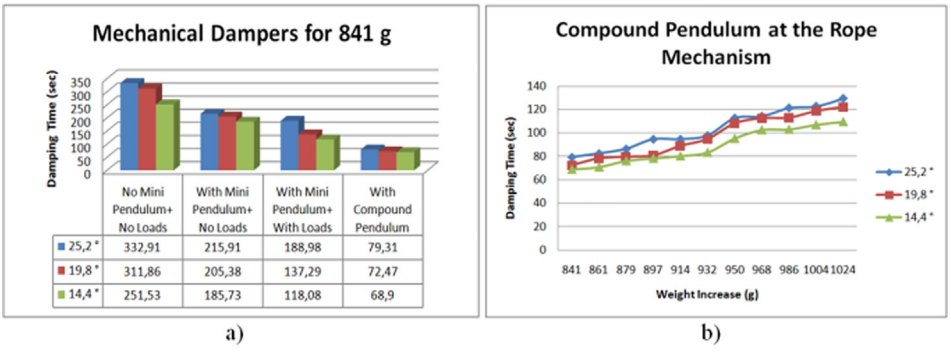

Fig.18 a) Damping times of the main pendulum with a rope at the different conditions and angles b) Damping times of the main pendulum with a rope and a compound pendulum with different weights and angles.

below link; https://drive.google.com/drive/folders/1Jwp5Jwz3pSTTTORtBU-JQCT59tdalXl?usp = sharing

3.4. Oscillation tests of compound pendulum with a rope

This pendulum has a rope mechanism instead of a steel bar. Next to this rope, two more ropes are attached from the left and right sides of the mini pendulum aiming to reach to the load being carried. The mini pendulum ropes pass under the drum as it enters the drum and is hugged to the drum from different directions. Thus, the main pendulum is subjected to more convenient and effective reverse forces. As shown in Fig. 18(a), the main pendulum is allowed to oscillate with the compound pendulum from different angles. Approximately seventy-seven percent (77%) damping times have been achieved. Here the tension values of the mini pendulum ropes

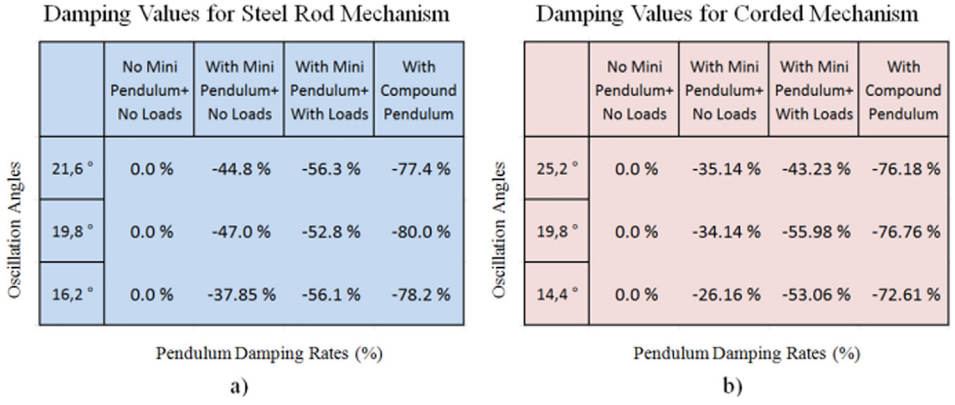

Fig.19 Damping rates of the main pendulum; a) with a steel rod and different pendulum dampers b) with a rope and different pendulum dampers.

Table 3 Damping rates due to oscillation and moment difference (Pos. I and II).

Pendulum with a Steel Rod			
	Pos. 0	Pos. I	Pos. II
	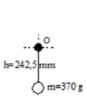	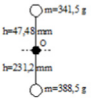	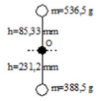
Moment Difference	0 %	18,05 %	50,97 %
Realized Oscillation Time for 21,6°	74,61 sec.	41,18 sec.	32,61 sec.
Expected Oscillation Time According to the Moment Difference for 21,6°	–	61,20 sec.	36,62 sec.
Time Gain Due to the Oscillation for 21,6°	–	32,71 %	10,95 %
Time Gain in Practise for 21,6° (Figure 19a)	–	44,80 %	56,30 %
Time Gain Due to the Moment Difference for 21,6°	–	12,09 %	45,35 %
Time Gain Due to the Oscillation for 19,8°	–	35,37 %	3,83 %
Time Gain Due to the Moment Difference for 19,8°	–	11,63 %	48,97 %
Time Gain Due to the Oscillation for 16,2°	–	24,24 %	10,58 %
Time Gain Due to the Moment Difference for 16,2°	–	13,61 %	45,52 %

Table 4 Damping rates due to oscillation and moment difference (Pos. III and IV).

Pendulum with a Rope			
	Pos. 0	Pos. III	Pos. IV
		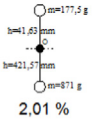	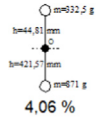
Moment Difference	0 %	2,01 %	4,06 %
Realized Oscillation Time for 25,2°	332,91 sec.	215,91 sec.	188,98 sec.
Expected Oscillation Time According to the Moment Difference for 25,2°	–	327,42 sec.	320,58 sec.
Time Gain Due to the Oscillation for 25,2°	–	34,06 %	41,05 %
Time Gain in Practise for 25,2° (Figure 19b)	–	35,14 %	43,23 %
Time Gain Due to the Moment Difference for 25,2°	–	1,08 %	2,18 %
Time Gain Due to the Oscillation for 19,8°	–	33,04 %	54,28 %
Time Gain Due to the Moment Difference for 19,8°	–	1,10 %	1,70 %
Time Gain Due to the Oscillation for 14,4°	–	24,92 %	51,25 %
Time Gain Due to the Moment Difference for 14,4°	–	1,24 %	1,81 %

Table 5 Damping rates due to oscillation and moment difference (Pos. V and VI).

Compound Pendulum with a Steel Rod		Compound Pendulum with a Rope	
Pos. V		Pos. VI	
		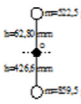	
Moment Difference	42,73 %	Moment Difference	8,95 %
Realized Oscillation Time for 21,6°	74,61 sec. for the no mini pendulum and no loads 16,89 sec.	Realized Oscillation Time for 25,2°	332,91 sec. for the no mini pendulum and no loads 79,31 sec.
Expected Oscillation Time According to the Moment Difference for 21,6°	45,77 sec.	Expected Oscillation Time According to the Moment Difference for 25,2°	303,80 sec.
Time Gain Due to the Oscillation for 21,6°	63,10 %	Time Gain Due to the Oscillation for 25,2°	73,89 %
Time Gain in Practise for 21,6° (Figure 19a)	77,40 %	Time Gain in Practise for 25,2° (Figure 19b)	76,18 %
Time Gain Due to the Moment Difference for 21,6°	14,30 %	Time Gain Due to the Moment Difference for 25,2°	2,29 %
Time Gain Due to the Oscillation for 19,8°	67,35 %	Time Gain Due to the Oscillation for 19,8°	74,54 %
Time Gain Due to the Moment Difference for 19,8°	12,65 %	Time Gain Due to the Moment Difference for 19,8°	2,22 %
Time Gain Due to the Oscillation for 16,2°	64,46 %	Time Gain Due to the Oscillation for 14,4°	69,98 %
Time Gain Due to the Moment Difference for 16,2°	13,74 %	Time Gain Due to the Moment Difference for 14,4°	2,63 %

also play an important role. It is estimated that these tension values affect the main load as it shares the load, resulting in more successful results.

As a result, oscillation plots obtained from mini pendulums have lower amplitudes (almost zero). During the experimental tests, the pendulum mace moved very little. These values were below $+0.36°/-0.36°$ degrees. Since the pulse value of the encoders is 200 units, these oscillation values could not be reflected in the graphs as shown in Fig. 17(d,e,f). Furthermore, the balancing weight above the peak of the main pendulum used to damp the oscillation. Compound pendulum performance was then tested with ten different weights and at three different angles. The test results are presented in Fig. 18(b). All graphic results can be seen at the belong link; https://drive.google.com/drive/folders/1Jwp5Jwz3pSTTTORtBU-JQCT59tdalXl?usp=sharing

4. Results and discussions

The aim of this study to reduce the workload of the crane operator and to develop a faster and safer crane transport system. Besides, alternative solutions have been developed for unexpected situations that may arise in the external environment. Increasing the number of connection support mechanisms such as extra supporting rope for wind loads provides many benefits to the systems. The only thing that needs to be considered here is that when the crane mechanism is in working position or standing at a fixed point, it is not clear which direction and intensity of the wind will blow. To avoid such problems, this mechanical damping system that changes direction against the wind will provide advantages in load positioning. The mechanical dampers in this study can rotate around 360° degrees.

Instead of installing directing wings to this system, an electrical motor, a wind direction sensor, and a microcontroller card can rotate the upper platform according to the wind direction. Also, the motion of the mini-damping pendulums can be controlled by electrical motors, sensors, and a microcontroller card instead of gravitational force for future studies.

Table 6a Crane automations in the private sector.

Ref.	Firm, System	Appl. Places	Control Skills
[52]	Liebherr, Cycoptronic	Rotary, Boom, Liebherr Harbour Mobile Cranes.	The automation concept, anti-sway, tracking control, and oscillation damping system.
[53]	BRITE-EURAM (Six European Partners)	Gantry Cranes.	A modular distributed control system for crane and hoist automation, anti-swing, condition monitoring, teleoperation, automatic load coupling/decoupling, and automatic cycling.
[54]	Mitsubishi Heavy Industries Ltd. (MHI)	Rail-Mounted Gantry Crane (RMGC), Rubber-Tired Gantry Cranes (RTGs).	High-accuracy stacking control technology and automatic traveling control technology for helping the crane to the target position. Automatic hoisting, trolley traveling, steering, and positioning control.
[55], [56]	Siemens Cranes, STS-cranes, AGV's and ARMG's.	Yard Cranes, Container Cranes, RTG, RMG, STS, GSU, OHBC, and Slewing Cranes.	Automation systems are essential to predict the performance of automated yard cranes. The newly developed yard crane model is used with automation and interconnecting elements on container terminals. Performance prediction and sensitivity analysis. A better solution performance estimation is provided to customers. Also, SIMOCRANE Sway Control Systems are among the works for automatic swing control for different types of cranes. With automatic swing control, the operator relaxes and the load is positioned faster and more accurately.
[57]	(ZPMC), COSCO Shipping Ports Limited	The Port Industry.	Operation manpower was reduced by about 85%, and operation efficiency was increased by about 30% by automated guided vehicles (AGVs), automated the equipments and control systems in Yangshan Port.
[58]	ABB Crane Systems	Yard Automation.	Sway control, positioning/path control, skew control, 4 directions: trolley, gantry, hoist positions. Precise positioning systems to minimize cycle time and efficient Crane Management System (CMS).

Table 6b Crane automations in the private sector.

Ref.	Firm, System	Appl. Places	Control Skills
[59]	Konecranes, ARTG System	16-wheel RTGs.	Active Load Control (ALC) system that eliminates container sway and enables automation thanks to ability about adapt to rough yard surfaces.
[60]	iSAM Group, Grab Unloader Automation System	Ship Unloaders.	Intelligent grab tracking system based on the 3D real-time laser scanner is one of the main features. The high-tech scanner track the crane ropes and the grab itself in real-time to measure sway and grab attitude. Data from the grab tracking system ensures a continuous update of the energy and position model for the grab's moving path. This enables a precise "landing" of the grab with a precision of about 0.5 m in almost all weather conditions. Hence less wear and tear occur in automatic mode.
[61]	PEMA, Container Terminal Automation	Rubber Tyred Gantry Cranes.	Today many manually operated rubber-tyred gantry cranes (RTGs) have automation systems. These systems are; automatic steering, anti-sway, spreader micro-motion, collision avoidance, truck positioning, automatic gantry and trolley positioning, and container PDS systems.
[62]	TMEIC, Maxspeed and Maxview Crane Systems	Rail Mounted Gantry Cranes.	The patented system reduces the sway of the spreader during load moves. In manual operation, the operator is sending a speed reference to catch the load as it swings. So manually catching the load is hard. In automatic operation with Sway Control, the system figures out how to catch the payload by controlling the speed of the spreader. The operation is faster since the trolley and load come to rest at the same time, without waiting for sway damping. The load is checked in one swing of the pendulum and does not overshoot the stop position. There is no need for hardware sensors and sway control can operate in the manual as well as in automatic moves. The trolley and gantry sway performance is ± 50 mm, which can be developed. Skewing sway is less than one degree and the system is cheap and more reliable than hydraulic anti-sway control systems.

Table 7 Mechanical damping methods in the private sector.

Ref.	Firm, System	Appl. Places	Control Skills
[63]	Liebherr of Killarney, Co. Kerry, Ireland.	Ship-to-Shore (STS) Cranes.	A novel tie-down system, incorporating equalizing beam and torque adjustable features, has been designed. This system is especially designed to prevent unequal tensile loads on the turnbuckles and consequent potential failure mechanisms, which for a ship to shore cranes can be life-threatening, function disruptive, crane/quay structure damaging and more costly. Extensive modeling and wind tunnel testing of airflow around critical sections indicated an optimal analysis method.
[58]	ABB, Konecranes	Gantry Cranes.	Trimming by independently controllable main hoist winches. When looking at the rope diagram, the system consists of Load Cells, Hoist Machinery, Auxiliary Winches, Pulleys of the Head Blocks. In this way, reeving and micro-motion can be done on the container. • Rope reeving: rope tower/straight ropes with sheaves. • Micro–motion: hydraulic/electric/auxiliary ropes. So the system is mechanically robust and allows operation in high winds.
[64]	Liebherr Container Cranes	Rubber Tyre Gantry Cranes.	Sway elimination is provided on the container with the eight rope reeving system. The eight rope reeving arrangement for the hoist as situated on the trolley provides payload oscillation is eliminated in the hoist, trolley, long travel, and skew directions. Combined with superior fine positioning for stack building and truck handling empowers for fertility increases of between 30 and 40% according to alternative designs.
[56]	Siemens, Simocrane CenSOR Camera Measuring System	Overhead Bridge Cranes/Gantry Cranes, Container Cranes STS/Grab Cranes GSU.	The SIMOCRANE Sway Control System is based on the a mathematical oscillation model. If a camera is used, the parameters hoisting height, swing angle, and rotation angle are determined using optical contact-free measurement and are used in the model. Damping of the load is performed by influencing the traversing speed for each axis individually. All swaying eliminated. If a camera is also used, swaying resulting from external forces – such as inclined lift or wind – can be completely compensated. Also, the sway neutralization (SNL/SND) mode (only for the version with a camera) is used to eliminate swaying movements of the payload from a standstill. Sway neutralization results in slight travel movements to both sides of the target position. The position of the payload is acquired by the camera measuring system. Furthermore, TLS control controls the trim, list, and skew positions of a spreader. The TLS control function assumes that • the length or • the pivot points of the 4 support cables of a spreader can be adjusted by hydraulic cylinders or an additional electric drive with the help of the camera.
[65]	Kalmar ASC System	Automatic Stacking Crane.	The cranes feature a redesigned machinery cart with Max Stable type stiff rope reeving. The rope tower is more compact but still maintains optimum stiffness for fast and accurate automated operation with easier rope replacement and adjustment procedures.
[66]	It Was Supported By the Ministry of Science andTech. of Korea	1/4-Size Rail-Mounted Quayside Pilot Crane, Real Rubber-Tired Gantry Crane.	Using the kinematics of the hoist reeving mechanism, a new sway-angle detection method using the inclinometer attached on the head block was suggested for the sway problem of container cranes with multiple ropes. To suppress the sway, a multivariable state feedback controller with an integrator was suggested. The developed sway-angle measurement method and control algorithm is very cost-effective and promising.

These motors can start damping the main pendulum earlier with various intelligent control methods. As a result, the damping ratios in Fig. 19 can be increased by such methods. Detailed damping rates for each position are listed in Tables 3, 4, and 5.

According to the values in Table 3, the most effective damping reason for Pos. I is due to oscillation. The effect because of the moment difference is less. When look at Pos II, the moment difference has the most impact on the damping rates. The reason for this situation is the weights added to both

sides of the pendulum. When look in Table 4, the most effective damping for Pos. III is due to the oscillation. The effect of moment difference is very small here. The tension values of the second and third ropes added to the system are also effective for this situation. Rope tensions are not kept high here. The same situation is also seen at Pos. IV. There is a slight increase in damping rates due to the weights added to the system. Especially in damping rates due to the moment difference. The damping increase here is due to oscillation. As seen in Table 5, the damping ratios of the compound pendulums are studied for Pos. V and Pos. VI. In both cases, the damping rates due to oscillation are relatively higher. At here, the amount of weights added to the mini pendulums are less than previous trials. The tension values of the second and third ropes added to the system in both positions are higher than the previous trials. Therefore, the damping rates due to oscillations are more effective. As a result, all trials have been examined at three different angle values and the importance of the compound pendulum in damping has been tried to be illustrated with tables.

As can be seen in Tables 6a and 6b, there are many operations on cranes can be carried out thanks to automation. The swing and precise positioning controls are the most widely applied methods. The hoist automation, automatic load coupling/ decoupling, and automatic cycling are other important automation methods. With these methods, operation manpower has been significantly reduced and operational efficiency has been increased. The benefits of automation, especially in port operations, are very important for the private sector. Also, many companies have developed alternative measurement methods to reduce automation costs in this sector. For example, performing swing control manually with automatic movements instead of hardware sensors. The aim is to provide the highest efficiency with the most effective and economical methods. In this article, the automation method is used to obtain system parameters quickly. Many companies share their control methods to a certain extent because they are commercial information. More information is given about patented systems.

When looked in Table 7, various mechanical damping methods were performed by the private sector. All these methods have been developed against wind forces in port cranes.

The studies focused more on ropes and their tensions. The payload swing was also aimed at minimizing. The benefits of adding additional ropes to the system mentioned in this article are also seen in private sector studies. These additional ropes are effective in precise positioning and load swings. The benefits of excessive rope tension used in the study is more common in container cranes.

5. Conclusion

In this study, both automation and mechanical damping methods are presented for a simple single pendulum system. Automated systems are indispensable methods for production processes. The topic is an area that needs to be constantly improved for more production and a safer working environment. In this study, an alternative automation block was developed to position different weights at different heights with a minimum swing. The current T values and ζ of the system could be calculated by releasing a loaded pendulum to free swing from the same height as the working angle. Later, this input data was reproduced and used in the hybrid control method consisting of ZV input shaping and NNs. Also, mechanical damping methods were developed primarily to absorb wind forces. It is accepted that the wind direction is parallel to the crane mechanism and the main pendulum from different heights was left for free swing. In the tests carried out, damping rates of up to 80% have been achieved. The mini pendulum oscillations acting in the opposite direction to the main pendulum swing played a more effective role in damping. It is thought that this damping rate can be increased even more with intelligent control methods, electric motors, and various sensors. Also, these absorbers have been thought to be prone to real practices.

6. Information

This study, which is not supported by any institution, belongs to the doctoral graduation project. Çukurova University, Institute of Natural and Applied Sciences, Department of Mechanical Engineering.

Declaration of Competing Interest

The authors declare that they have no known competing financial interests or personal relationships that could have appeared to influence the work reported in this paper.

References

[1] Meb, Education notes, 2019, https://www.megep. meb.gov.tr.
[2] S. Garrido, M. Abderrahim, A. Giménez, R. Diez, C. Balaguer, Anti-swinging input shaping control of an automatic construction crane, IEEE Trans. Autom. Sci. Eng. 5 (3) (2008), https://doi.org/10.1109/TASE.2007.909631.
[3] H. Aschemann, O. Sawodny, E.P. Hofer, Active damping of tilt oscillations and trajectory control of overhead cranes, IEEE, 2000, 0-7803-64562/00/$ 10.00.
[4] S. Lahres, H. Aschemann, O. Sawodny, E.P. Hofer, Crane automation by decoupling control of a double pendulum using two translational actuators, AACC, 2000, 0-7803-55199/00 $10.00. https://doi.org/10.1109/ACC.2000.876661.
[5] H. Ying, G. Yang, H. Lan, L. Yunbo, Design and implementation of a multifunctional self-balancing mobile platform, IEEE (2015) 978-1-4799-70162/15 /$31.00. https://doi.org/10.1109/CCDC.2015.7161818.
[6] S. Ozana, M. Pies, R. Hajovsky, Computation of swing-up signal for inverted pendulum using dynamic optimization, in: IFIP International Federation for Information Processing CISIM, LNCS 8838 (2014) 301-314. https://doi.org/10.1007/978-3-662-45237-0_29
[7] P. Seman, M. Juhás, L. Tkáč, M. Honek, New possibilities of industrial programming software, IEEE (2013) 978-1-4799-0927-8/13/$31.00. https://doi.org/10.1109/PC.2013.6581456.
[8] N. Semenič, A. Sarjaš, R. Svečko, A. Chowdhury, Design and implementation of rapid control prototyping system with Matlab/Simulink, Informacije MIDEM 41 (2) (2011) 122–131.
[9] T.T. Dos Santos, M.C. Magnus, C.C. Scharlau, J.F. Haffner, L. F.A. Pereira, A decentralized control of inverted pendulum and supervision based on internet tools, IEEE (2003) 0-7803-79063/03/$17.00. https://doi.org/10.1109/IECON.2003.1280647.
[10] A. Ghafooripour, H. Kiamehr, An overview of system identification methods and applications, Part I: methods of system identification and dynamic tests, in: 4th international

conference on coasts, ports & marine structure, Shahid Rajaee Port Complex, Bandar Abbass, 2000.
[11] B. Haznedar, A. Kalinli, Training ANFIS structure using simulated annealing algorithm for dynamic systems identification, Neurocomputing 302 (2018) 66–74, https://doi.org/10.1016/j.neucom.2018.04.006.
[12] S. Kirkpatrick, C.D. Gelatt, M.P. Vecchi, Optimization by simulated annealing, Science 220 (1983) 671–680, https://doi.org/10.1126/science.220.4598.671.
[13] L. Ljung, Perspectives on system identification, Ann. Rev. Control 34 (2010) 1–12, https://doi.org/10.1016/j.arcontrol.2009.12.001.
[14] T.A. Tutunji, Parametric system identification using neural networks, Appl. Soft Comput. 47 (2016) 251–261, https://doi.org/10.1016/j.asoc.2016.05.012.
[15] S.S. Gürleyük, Dinamik Sistemler, Kontrol ve Giriş Şekillendirici Denetim, Palme Yayıncılık, Ankara, 2015.
[16] I. Maharıq, A. Ercıyas, A spectral element method for the solution of magnetostatic fields, Turkish J. Electr. Eng. Comput. Sci. (2017) 25: 2922–2932. https://doi:10.3906/elk-1605-6.
[17] I. Mahariq, H. Kurt, M. Kuzuoğlu, Questioning degree of accuracy offered by the spectral element method in computational electromagnetics, ACES J. 30 (7) (2015) 698–705. Corpus ID: 62835266
[18] I. Mahariq, On the application of the spectral element method in electromagnetic problems involving domain decomposition, Turkish J. Electr. Eng. Comput. Sci. 25 (2017) 1059–1069, https://doi.org/10.3906/elk-1511-115.
[19] I. Mahariq, M. Kuzuoğlu, I.H. Tarman, H. Kurt, Photonic nanojet analysis by spectral element method, IEEE Photon. J. 6 (5) (2014) 6802714, https://doi.org/10.1109/JPHOT.2014.2361615.
[20] I. Mahariq, M. Kuzuoğlu, I.H. Tarman, On the attenuation of the perfectly matched layer in electromagnetic scattering problems with the spectral element method, ACES J. 29 (9) (2014) 701–710. Corpus ID: 64629771.
[21] I. Mahariq, H. Kurt, Strong field enhancement of resonance modes in dielectric microcylinders, J. Opt. Soc. Am. B 33 (4) (2016) 656–662, https://doi.org/10.1364/JOSAB.33.000656.
[22] I. Mahariq, H.I. Tarman, M. Kuzuoğlu, On the accuracy of spectral element method in electromagnetic scattering problems, Int. J. Comput. Theory Eng. 6 (6) (2014) 495–499, https://doi.org/10.7763/IJCTE.2014.V6.916.
[23] H. Yavuz, S. Beller, An intelligent serial connected hybrid control method for gantry cranes, Mech. Syst. Sig. Process. 146 (2021), https://doi.org/10.1016/j.ymssp.2020.107011 107011.
[24] A.H. Nayfeh, Z.N. Masoud, N.A. Nayfeh, A delayed-position feedback controller for cranes, in: IUTAM Symposium on Chaotic Dynamics and Control of Systems and Processes in Mechanics, Springer, 2005, 385–395. https://doi.org/10.1007/1-4020-3268-4_36.
[25] Q.H. Ngo, K.-S. Hong, Sliding-mode antisway control of an offshore container crane, IEEE/ASME Trans. Mechatron. 17 (2) (2012), https://doi.org/10.1109/TMECH.2010.2093907.
[26] K.L. Sorensen, W. Singhose, S. Dickerson, A controller enabling precise positioning and sway reduction in bridge and gantry cranes, Control Eng. Pract. 15 (2007) 825–837, https://doi.org/10.1016/j.conengprac.2006.03.005.
[27] J. Huang, E. Maleki, W. Singhose, Dynamics and swing control of mobile boom cranes subject to wind disturbances, IET Control Theory Appl. 7 (9) (2013) 1187–1195. https://doi.org/10.1049/iet-cta.2012.0957.
[28] J.-H. Suh, J.-W. Lee, Y.-J. Lee, K.-S. Lee, Anti-sway position control of an automated transfer crane based on neural network predictive PID controller, J. Mech. Sci. Technol. 19 (2) (2005) 505–519, https://doi.org/10.1007/BF02916173.
[29] S. Pezeshki, M.A. Badamchizadeh, A.R. Ghiasi, S. Ghaemi, Control of overhead crane system using adaptive model-free and adaptive fuzzy sliding mode controllers, J. Control Autom. Electr. Syst. 26 (2015) 1–15, https://doi.org/10.1007/s40313-014-0152-4.
[30] K.-T. Hong, C.-D. Huh, K.-S. Hong, Command shaping control for limiting the transient sway angle of crane systems, Int. J. Control Autom. Syst. 1 (1) (2003).
[31] M.-C. Pai, Closed-loop input shaping control of vibration in flexible structures via adaptive sliding mode control, Shock Vib. 19 (2012) 221–233, https://doi.org/10.1155/2012/803479.
[32] A.M. Abdullahi, Z. Mohamed, H. Selamat, H.R. Pota, M.S.Z. Abidin, F.S. Ismail, A. Haruna, Adaptive output-based command shaping for sway control of a 3D overhead crane with payload hoisting and wind disturbance, Mech. Syst. Sig. Process. 98 (2018) 157–172, https://doi.org/10.1016/j.ymssp.2017.04.034.
[33] V. Duc La, Crane sway reduction using coriolis force produced by radial spring and damper, J. Mech. Sci. Technol. 29 (3) (2015) 973–979, https://doi.org/10.1007/s12206-015-0211-1.
[34] V. Duc La, Y. Park, A Cable-Passive Damper System for Sway and Skew Motion Control of a Crane Spreader, Hindawi Publishing Corporation Shock and Vibration Volume, ID 507549 (2015) 11. https://doi.org/10.1155/2015/507549.
[35] S.-T. Park, T.-T. Luu, A new method for reducing the natural frequency of single degree of freedom systems, J. Sound Vib. 300 (2007) 422–428, https://doi.org/10.1016/j.jsv.2006.08.017.
[36] V.S. Aslanov, Stability of a pendulum with a moving mass: the averaging method, J. Sound Vib. 445 (2019) 261–269, https://doi.org/10.1016/j.jsv.2019.01.021.
[37] A. Arena, W. Lacarbonara, A. Casalotti, Payload oscillations control in harbor cranes via semi-active vibration absorbers: modeling, simulations and experimental results, Procedia Eng. 199 (2017) 501–509, https://doi.org/10.1016/j.proeng.2017.09.136.
[38] B. Balachandran, Y.-Y. LI, A mechanical filter concept for control of non-linear crane-load oscillations, J. Sound Vibration 228(3) (1999) 651–682. https://doi.org/10.1006/jsvi.1999.2440.
[39] G. Hurel, A.T. Savadkoohi, C.-H. Lamarque, Nonlinear vibratory energy exchanges between a two degrees-of-freedom pendulum and a nonlinear absorber, J. Eng. Mech., Am. Soc. Civ. Eng. 145-(8), (2019). https://doi.org/10.1061/(ASCE)EM.1943-7889.000 1620
[40] J. Awrejcewicz, N. Losyeva, V. Puzyrov, Pervasive damping in mechanical systems and the role of gyroscopic forces, Z Angew Math Mech. 99 (2019), https://doi.org/10.1002/zamm.201800119 e201800119.
[41] T. Yuen, L. Balan, M. Mehrtash, Implementation of an absorber design for vibration control in automation systems, Procedia Manuf. 32 (2019) 578–584, https://doi.org/10.1016/j.promfg.2019.02.255.
[42] D. Taguchi, R. Sakaguchi, T. Sugiura, Vibration reduction of a high-T_c superconducting magnetic levitation system with an autoparametric vibration absorber, IEEE Trans. Appl. Supercon ductivity 21 (3) (2011), https://doi.org/10.1109/TASC.2010.2091246.
[43] S.-T. Wu, Y.-R. Chen, S.-S. Wang, Two-degree-of-freedom rotational-pendulum vibration absorber s, J. Sound Vib. 330 (2011) 1052–1064, https://doi.org/10.1016/j.jsv.2010.09.028.
[44] L. Collini, R. Garziera, K. Riabova, M. Munitsyna, A. Tasora, Oscillations control of rocking-block-type buildings by the addition of a tuned pendulum, Hindawi Publishing Corporation, Shock and Vibration Volume, ID 8570538 (2016) 11. https://doi.org/10.1155/2016/8570538.
[45] Pololu, Brushed DC motor, 2018. https://www.pol olu.com/product /3213.
[46] Pololu, Motor controller card, 2018. https://www. pololu.com/product/1383.
[47] Sparkfun, Rotary encoder, 2019. https://static.sparkfun.com/datasheets/Robotics/E6A2%20encoder.pdf.

[48] Humusoft, Data acquisition card, 2018. https://ww w.humusoft.cz/ datacq/mf634/.
[49] K. Ogata, System Dynamics, Fourth Edition., Pearson Education, 2013.
[50] S. Bayari, 2020. The dynamic equilibrium method education notes, http://yunus.hacettepe.edu.tr/~ba yari/FZO%20301%20Titresim%20ve%20Dalgalar/BOLUM-3-Y.pdf.
[51] Tobb Etü, 2020. The dynamic equilibrium method education notes, http://fizikservis.etu.edu.tr/ders16.pdf.
[52] O. Sawodny, J. Neupert, E. Arnold, Actual trends in crane automation – directions for the future, FME Trans. 37 (2009) 167–174.
[53] N.A. Armstrong, P.R. Moore, R.H. Weston, Generic Crane and Hoist Automation with the Application of Advanced Control Architectures, Automation and Robotics in Construction X, Elsevier Science Publishers B.V., 1993. http://dx.doi.org/10.22260/ISARC1993/0013
[54] K. Obata, K. Uchida, T. Chikura, H. Yoshikawa, T. Monzen, Automated Transfer Crane, Mitsubishi Heavy Industries, Ltd. Technical Review, 2003, Vol.40 E. No.2.
[55] N.T. Jongbloed, Performance Prediction Model for Automated Container Yard Cranes, Delft University of Technology, Masters thesis, Report number: 2018.TEL.8294.
[56] Siemens, Catalog CR1-Edition 2015, 2020, https://assets.new.siemens.com/siemens/assets/api/uuid:94885b35-d35646a7aa28e1e7092009d1/ version:1563778309/siemens-cranes-catalog-cr.pdf.
[57] Huawei, Smart Port 2019, 5G Smart Port White Paper, 2020, https://www-file.huawei.com//media/ corporate/pdf/xlab/2019/5gsmartportwhitepaperen.pdf?la = en.
[58] ABB, Equipment for Yard Automation, AAPA Facilities Engineering Seminar 2007, 2020, https://www.aapa-ports.org/files/seminarpresentati ons/07facengcederqvisthans.pdf.
[59] Konecranes, Brochure, The Yard Revolution Automated RTG, 2020, https://pdf.directindustry. com/pdf/konecranes/automated-rtg/16156-603037.html.
[60] iSAM Group, Brochure, Automation of Grab Ship Unloaders (GSU) for Bulk Materials, 2020, https://www.isam-ag.de/wpcontent/uploads/ENAp plikReportAutomation-of-GSUs.pdf.
[61] Pema, A PEMA Information Paper 2016, Container Terminal Automation, 2020, https://www.pema.org/wp-content/uploads/downlo ads/2016/06/PEMA-IP12-Container-Terminal-Auto mation.pdf.
[62] Tmeic, Brochure 2011, Crane Control and Automation Global Solutions, 2020, https://www. tmeic.com/Repository/Others/TMG-1424%20Cran e%20Control%20Industry-Mar2015-lores.pdf.
[63] B. Hand, Final Year Capstone Project, An Analysis into Wind Induced Loading Effects on a Ship-to-Shore (STS) Crane and Investigation into Design Optimisation, 2020, https://issuu.com/mycit/docs/ brian_hand_essay_ship_to_shore_equa.
[64] Liebherr Container Cranes, Brochure, Rubber Tyre Gantry Cranes, 2020, http://www.macport.it/archi vio/22/53-liebherr-rtg-cranesbrochure.pdf.
[65] Kalmar, Brochure 2015, Next generation Kalmar ASC system, (2020) https://www.kalmar.fi/49297a/globalassets/equipment/automatedstacking-cranes /the-next-generation-kalmar-asc-system.pdf.
[66] Y.-S. Kim, K.-S. Hong, S.-K. Sul, Anti-sway control of container cranes: inclinometer, observer, and state feedback, Int. J. Control, Automation, Syst. 2 (4) (2004) 435–449.